Inorganic Chemistry
Cite This: Inorg. Chem. XXXX, XXX, XXX−XXX
Forum Article
pubs.acs.org/IC

endo-Hydroxamic Acid Monomers for the Assembly of a Suite of Non-native Dimeric Macrocyclic Siderophores Using Metal-Templated Synthesis

Christopher J. M. Brown,[†] Michael P. Gotsbacher,[†] Jason P. Holland,[‡] and Rachel Codd*[,†]

[†]School of Medical Sciences (Pharmacology), The University of Sydney, 2006 Sydney, New South Wales, Australia
[‡]Department of Chemistry, University of Zurich, Winterthurerstrasse 190, 8057 Zurich, Switzerland

Supporting Information

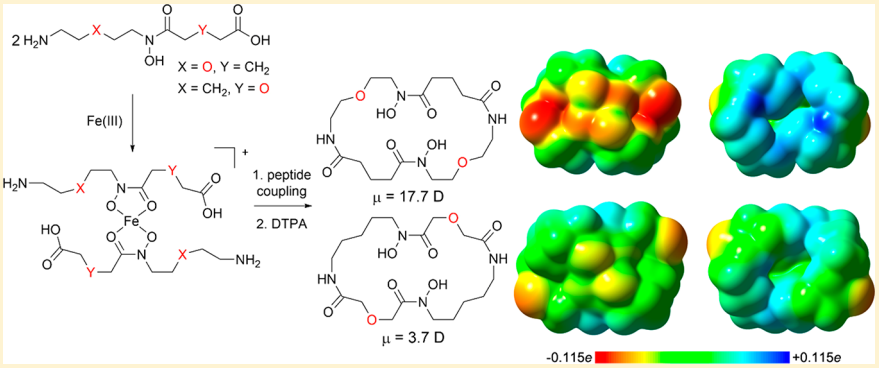

ABSTRACT: An expedited synthesis of *endo*-hydroxamic acid aminocarboxylic acid (*endo*-HXA) compounds has been developed. These monomeric ligands are relevant to the synthesis of metal−macrocycle complexes using metal-templated synthesis (MTS), and the downstream production of apomacrocycles. Macrocycles can display useful drug properties and be used as ligands for radiometals in medical imaging applications, which supports methodological advances in accessing this class of molecule. Six *endo*-HXA ligands were prepared that contained methylene groups, ether atoms, or thioether atoms in different regions of the monomer (**1**−**6**). MTS using a 1:2 Fe(III)/ligand ratio furnished six dimeric hydroxamic acid macrocycles complexed with Fe(III) (**1a**−**6a**). The corresponding apomacrocycles (**1b**−**6b**) were produced upon treatment with diethylenetriaminepentaacetic acid (DTPA). Constitutional isomers of the apomacrocycles that contained one ether oxygen atom in the diamine-containing (**2b**) or dicarboxylic acid-containing (**3b**) region were well resolved by reverse-phase high-performance liquid chromatography (RP-HPLC). Density functional theory calculations were used to compute the structures and solvated molecular properties of **1b**−**6b** and showed that the orientation of the amide bonds relative to the pseudo-C_2 axis was close to parallel in **1b**, **2b**, and **4b**−**6b** but tended toward perpendicular in **3b**. This conformational constraint in **3b** reduced the polarity compared with **2b**, consistent with the experimental trend in polarity observed using RP-HPLC. The improved synthesis of *endo*-HXA ligands allows expanded structural diversity in MTS-derived macrocycles and the ability to modulate macrocycle properties.

INTRODUCTION

Almost all bacteria produce low-molecular-weight organic ligands known as siderophores that have a high affinity toward Fe(III).[1−6] The formation of Fe(III)-siderophore complexes occurs as the first step in siderophore-mediated bacterial Fe acquisition, which serves to increase the availability of insoluble Fe(III) to bacteria, essential for survival.[7−10] Because of evolutionary pressure, a vast array of siderophores are produced with different molecular structures.[4] A large subset of siderophores contain the hydroxamic acid functional group as the Fe(III) binding motif. Trimeric hydroxamic acid siderophores form hexadentate 1:1 complexes with Fe(III) and include linear desferrioxamine B (DFOB) and macrocyclic desferrioxamine E (DFOE).[11−13] Dimeric hydroxamic acid macrocyclic siderophores isolated from nature include putrebactin, avaroferrin, bisucaberin, and alcaligin (Chart 1). These tetradentate macrocycles form 2:3 Fe(III)/ligand complexes at pH 7 and 1:1 complexes at acidic pH values[14−21] and can form complexes with other metal ions, including V(V), Mo(VI), and Cr(V).[18,21−23] Bisucaberin has been shown to have anticancer potential through Fe(III) deprivation mechanisms,[19] which provides the impetus to explore methods beyond total synthesis[24] to improve access to these types of molecules and to allow increased structural diversity. This is in

Special Issue: Metals in Biology: From Metallomics to Trafficking
Received: March 27, 2019

DOI: 10.1021/acs.inorgchem.9b00878
Inorg. Chem. XXXX, XXX, XXX−XXX

Chart 1. Dimeric Hydroxamic Acid Macrocyclic Siderophores Characterized from Nature

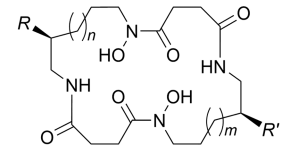

$n = m = 0$, $R = R' = H$	putrebactin
$n = 0$, $m = 1$, $R = R' = H$	avaroferrin
$n = m = 1$, $R = R' = H$	bisucaberin
$n = m = 0$, $R = R' = OH$	alcaligin

accordance with the broader potential of macrocycles as useful drug leads and inhibitors of protein−protein interactions,[25−30] which underpins developments in macrocycle synthesis.

Metal-templated synthesis (MTS) from *endo*-hydroxamic acid aminocarboxylic acid (*endo*-HXA) monomers has been used to furnish a range of dimeric,[31] trimeric,[32,33] or tetrameric[34] hydroxamic acid macrocycles. In a different approach, trimeric macrocyclic hydroxamic acid siderophores have been produced using Fe(III)-mediated macrolactonization of a preassembled linear trimer.[35] Trimeric DFOE was first produced using an MTS approach from a 1:3 complex formed in situ between Fe(III) and the *endo*-HXA monomer 4-[(5-aminopentyl)(hydroxy)amino]-4-oxobutanoic acid (PBH).[32] The flanking amino and carboxylic acid groups of contiguous PBH ligands were favorably positioned around the Fe(III) template for ring closure using diphenylphosphoryl azide (DPPA)-mediated peptide coupling. Ring-expanded analogues of trimeric DFOE were subsequently generated using MTS with the replacement of PBH with *endo*-HXA monomers that contained additional methylene groups in the diamine- or carboxylic acid-containing region of the ligand.[33] In a given MTS system, the nature of the metal ion template, the *endo*-HXA, and the reaction stoichiometry can direct the architecture of the terminal macrocycle. The use of Zr(IV) (typical coordination numbers in the range 6−8)[36,37] and the *endo*-HXA monomer 5-[(5-aminopentyl)(hydroxy)amino]-5-oxopentanoic acid (PPH) in a 1:4 ratio furnished a tetrameric hydroxamic acid macrocycle that saturated the Zr(IV) octadentate coordination sphere.[34] A selection of natural product dimeric hydroxamic acid macrocycles have been generated by MTS using a 1:2 Fe(III)/ligand reaction stoichiometry.[31]

One shortcoming of MTS in generating new macrocycles is the availability of the *endo*-HXA monomers. The existing literature syntheses[38,39] provide monomers in modest yields (about 10 mg per 5 days of synthetic undertaking), which can hinder progress in exploring the subsequent MTS chemistry. Our interest in increasing the traction of MTS for producing macrocycles tailored toward a given metal ion prompted us to reexamine the synthesis of *endo*-HXA monomers. In this work, we describe an expedited synthesis of *endo*-HXA monomers that gives significantly greater yields of product and uses a class of starting reagents that allow expansion of the structural diversity. The library of new *endo*-HXA monomers described here has been used in an MTS approach to generate a set of structurally diverse dimeric hydroxamic acid macrocycles, which have been characterized as holo (Fe(III)-loaded) complexes and apo (Fe(III)-free) ligands. These results provide the potential to expand MTS to generate new macrocycles with structures that deviate beyond those of natural products.

Scheme 1. Previous Syntheses of the Archetypal *endo*-HXA Monomer PBH via Route a[38,40,41] or b[39a]

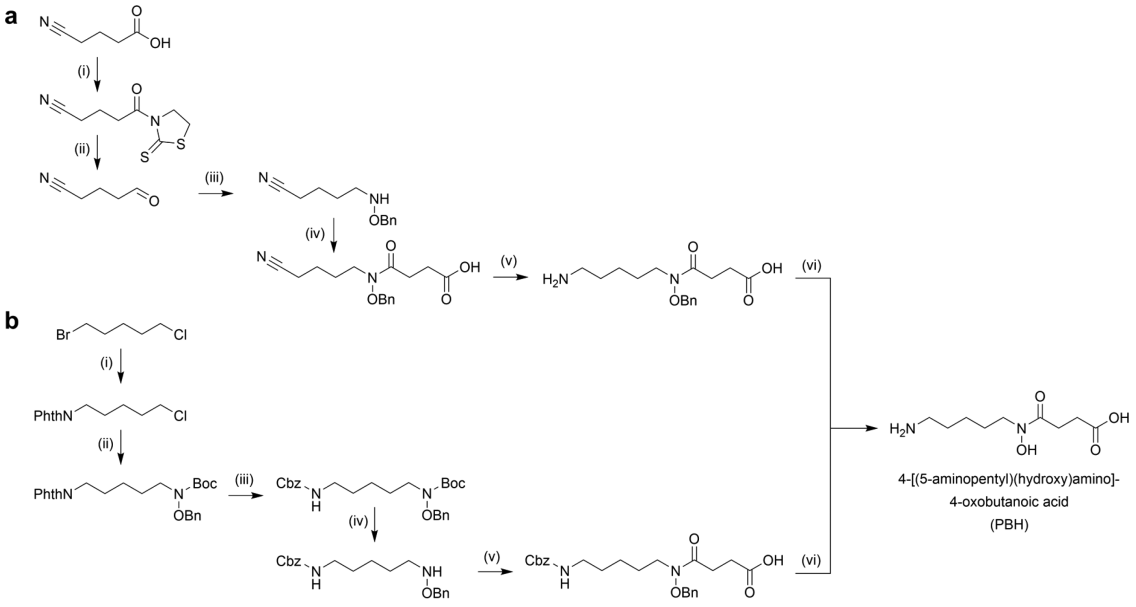

[a]Conditions (a): (i) thiazolidine-2-thione, CH_2Cl_2, Et_3N, 2-chloro-1-methylpyridinium iodide, rt, 24 h, yield not specified; (ii) diisobutylaluminum hydride, toluene, −78 °C, 2 h, then −40 °C, 3 h, 61%: (iii) BnO-NH_3Cl, H_2O, MeOH, KOH, 0 °C, 1 h, then $NaBH_3CN$, HCl in MeOH, rt, 3 h, 84%; (iv) succinic anhydride, pyridine, 100 °C for 1.5 h, then rt overnight, 98%; (v) H_2/Raney Ni/NH_3/MeOH, 0 °C, 3 h, 90%; (vi) H_2, 10% Pd/C, MeOH, HCl, rt, 3 h, 23%; (b): (i) potassium phthalimide, DMF, rt, 20 h, 84%; (ii) BnO-NH-Boc, NaH, NaI, DMF, 85 °C, 19 h, 82%; (iii) NH_2NH_2, EtOH, 90 °C, 3 h; CbzCl, H_2O, 1,4-dioxane, 0−20 °C, 12 h, 85% (two steps); (iv) 20% TFA, 20 °C, 2 h, 76%; (v) succinic anhydride, pyridine, 100 °C, 2 h, then 20 °C for 12 h, 72%; (vi) H_2, 10% Pd/C, ^{t}BuOH, 1,4-dioxane, HCl, rt, 3 h, 100%.

DOI: 10.1021/acs.inorgchem.9b00878
Inorg. Chem. XXXX, XXX, XXX−XXX

Scheme 2. Improved Synthesis of *endo*-HXA Monomers 1−6[a]

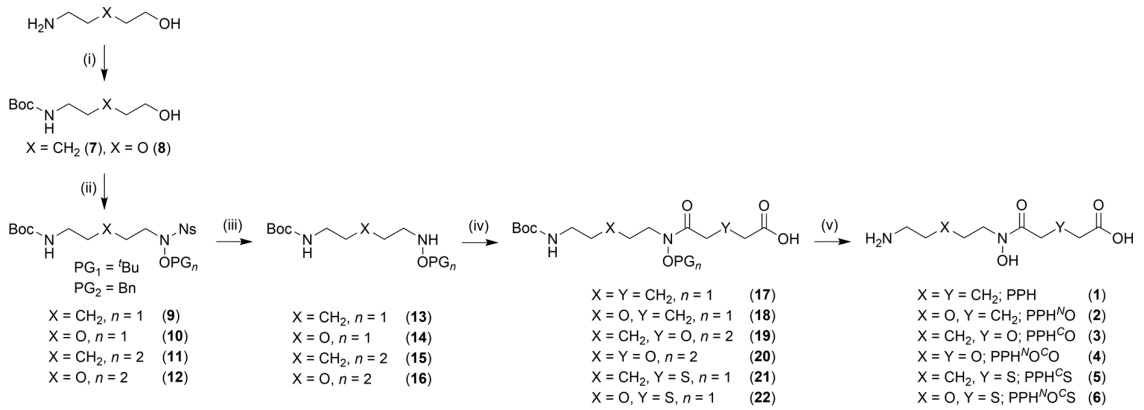

[a]Conditions: (i) Boc_2O, Et_3N, DCM, rt, 4 h; (ii) ^{t}BuO-NH-Ns (n = 1) or BnO-NH-Ns (n = 2), Ph_3P, DIAD, THF, 40 °C, 8 h; (iii) 2-mercaptoethanol, DBU, DMF, rt, 3 h; (iv) glutaric anhydride (**1** and **2**), 1,4-dioxane-2,6-dione (**3** and **4**), or 1,4-oxathiane-2,6-dione (**5** and **6**), DCM, rt, 3 h; (v) 9:1 TFA/DCM, rt, 4 h (n = 1) or 1:9 TFA/DCM, rt, 2 h; H_2, 10% Pd/C, ^{t}BuOH, 60 °C, 0.5 h (two steps; n = 2). PG_1 was used for **1**, **2**, **5**, and **6**. PG_2 was used for **3** and **4**.

RESULTS AND DISCUSSION

Synthesis of *endo*-HXA Monomers. The first described synthesis of PBH undertook a reaction between *O*-benzyl-*N*-(4-cyanobutyl)hydroxylamine and succinic anhydride, followed by nitrile-to-amine reduction (Raney Ni) and *O*-benzyl deprotection (H_2 over Pd/C).[38,40,41] The reaction conditions were harsh and furnished PBH in an overall yield of about 10% (Scheme 1a). A subsequent synthetic scheme used milder conditions[39] and has been widely adopted by others,[31,33,34,42] although the route is time-intensive and provides modest yields of about 32% (Scheme 1b).

The current work sought to improve the synthetic route toward *endo*-HXA monomers at the level of yield, number of steps, reaction times, and product diversity and are discussed with reference to PBH. First, the more commonly used starting reagent (Scheme 1b) 1,5-dibromopentane or 1-bromo-5-chloropentane was replaced with 1-amino-5-pentanol (Scheme 2). The initial stage of installation of the hydroxamic acid group involved the reaction between *N*-Boc-1-amino-5-pentanol and either *O*-*tert*-butyl-*N*-(2-nitrophenylsulfonyl)-hydroxylamine or *O*-benzyl-*N*-(2-nitrophenylsulfonyl)-hydroxylamine under Mitsunobu conditions.[43,44] The 2-nitrophenylsulfonyl (nosyl) N-protecting group was selected because it could be removed under mild conditions with a thiolate in a fashion orthogonal to the *O*-(*tert*-butyl)-*N*-alkylhydroxylamine (Scheme 2, PG_1) and *O*-benzyl-*N*-alkylhydroxylamine (Scheme 2, PG_2) protecting group systems.[43−45] Following the reaction with succinic anhydride to complete installation of the hydroxamic acid group, PBH could be generated from the *O*-*tert*-butyl-protected intermediate upon global deprotection with trifluoroacetic acid (TFA) or from the *O*-benzyl-protected intermediate with removal of the *N*-Boc group with dilute TFA followed by hydrogenation over Pd/C. The intermediates were readily purified using autoflash chromatography, with the purity increasing from **13**−**16** (80%) to **17**−**22** (95%) to **1**−**6** (95%).

The new synthetic path gave an overall yield (Scheme 2) of 49% and an overall reaction time for five (PG_1) or six (PG_2) steps of about 24 h. This compared to an overall yield of 10% and 65 h (six steps) for the earliest devised synthesis (Scheme 1a)[38,40,41] or 32% and 75 h (seven steps) for the more recent synthesis (Scheme 1b).[39] In addition to gains in the synthetic efficiency, the new route allowed for expanded structural diversity because of the availability of different types of amino alcohol start reagents.

This work focused on PPH as the primary *endo*-HXA monomer, which has been used successfully in previous MTS approaches. PPH contains an additional methylene group in the dicarboxylic acid-containing region than PBH and is prepared by replacing succinic anhydride with glutaric anhydride (PPH, **1**). The replacement of 1-amino-5-pentanol with 2-(2-aminoethoxy)ethanol gave a PPH analogue with an ether oxygen atom in the diamine-containing region (PPH^NO, **2**). A thioether atom could be introduced to the diamine-containing region using 2-[(2-aminoethyl)thio]ethanol as the start reagent, although this was not pursued here in order to maintain a reasonable scope of workload. The replacement of glutaric anhydride with 1,4-dioxane-2,6-dione or 1,4-oxathiane-2,6-dione gave PPH analogues containing an ether (PPH^CO, **3**) or thioether (PPH^CS, **5**) atom in the dicarboxylic acid-containing region. Replacements in both the diamine- and dicarboxylic acid-containing regions gave *endo*-HXA ligands containing variable substitutions of ether and thioether groups (PPH^NO^CO, **4**; PPH^NO^CS, **6**; Scheme 2).

Use of the *O*-*tert*-butyl protecting group for hydroxamic acid was first pursued as a general method for *endo*-HXA ligands because this could potentially enable global deprotection of the N−O^{t}Bu and NH−Boc groups with high concentrations of TFA. However, similar to observation from others,[44] in some instances the high concentration of TFA promoted hydrolysis of the hydroxamic acid group. This reactivity was dependent upon the nature of the anhydride employed in the reaction. The N−O^{t}Bu protecting group strategy was incompatible with 1,4-dioxane-2,6-dione but was compatible with glutaric anhydride and 1,4-oxathiane-2,6-dione. This was fortuitous in the case of 1,4-oxathiane-2,6-dione because this mitigated issues with sulfur poisoning of the catalyst in the Pd/C reductive deprotection route. The 1,4-dioxane-2,6-dione system required the use of a N−OBn protecting group, necessitating a two-step deprotection procedure (Scheme 2, step v). The instability of ether-containing molecules toward N−O^{t}Bu deprotection has been reported.[44] All *endo*-HXA ligands **1**−**6** were characterized using ^{1}H and ^{13}C, ^{1}H−^{1}H

DOI: 10.1021/acs.inorgchem.9b00878
Inorg. Chem. XXXX, XXX, XXX−XXX

Scheme 3. Synthesis of Dimeric Hydroxamic Acid Macrocycles as Fe(III) Complexes (Holomacrocycles 1a−6a) or as Free Ligands (Apomacrocycles 1b−6b)

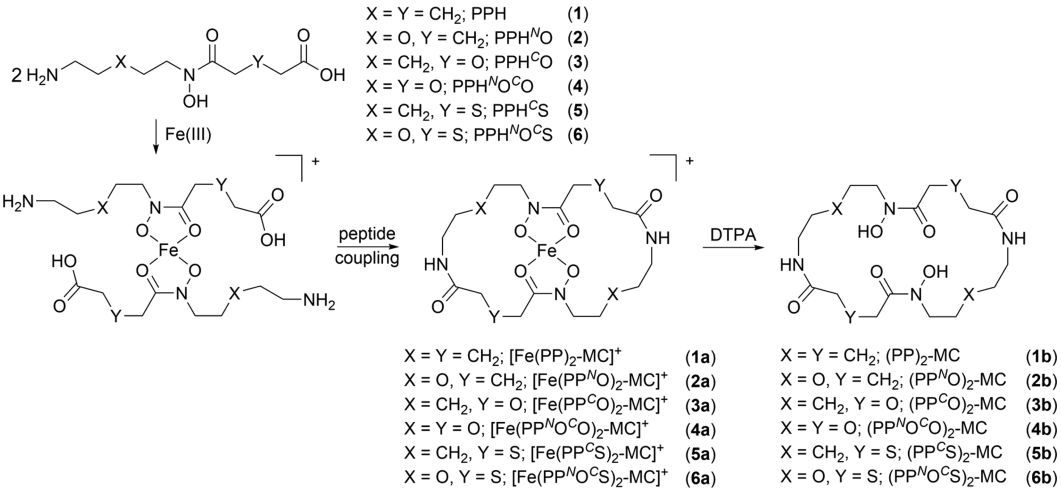

Table 1. HPLC Retention Times for Holomacrocycles 1a−6a and Apomacrocycles 1b−6b

holomacrocycle		t_R (min)	m/z_{exp}	apomacrocycle		t_R (min)	m/z_{exp}	*c* log P^a	*c* log P^b
$[Fe(PP)_2\text{-MC}]^+$	**1a**	21.0	482.2	$(PP)_2$-MC	**1b**	27.6	429.1	−2.84	0.64
$[Fe(PP^NO)_2\text{-MC}]^+$	**2a**	20.9	486.2	$(PP^NO)_2$-MC	**2b**	21.4	433.4	−5.93	−0.71
$[Fe(PP^CO)_2\text{-MC}]^+$	**3a**	25.8	486.2	$(PP^CO)_2$-MC	**3b**	29.7	433.3	−5.12	−1.48
$[Fe(PP^NO^CO)_2\text{-MC}]^+$	**4a**	21.4	490.2	$(PP^NO^CO)_2$-MC	**4b**	17.9	437.2	−8.21	−3.61
$[Fe(PP^CS)_2\text{-MC}]^+$	**5a**	30.4	518.2	$(PP^CS)_2$-MC	**5b**	30.2	465.2	−3.47	−0.40
$[Fe(PP^NO^CS)_2\text{-MC}]^+$	**6a**	22.4	522.1	$(PP^NO^CS)_2$-MC	**6b**	22.9	469.3	−6.56	−2.53

[a]Calculated using *ACD/ChemSketch 2017.2.1*. [b]Calculated using *Molinspiration* (https://www.molinspiration.com/cgi-bin/properties).

COSY, and $^1H-^{13}C$ HSQC NMR spectroscopy and high-resolution mass spectrometry (HRMS; Figures S1−S6).

Synthesis of Fe(III)-Loaded Macrocycles 1a−6a Using MTS. The set of *endo*-HXA monomers **1**−**6** allowed examination of the synthesis of new hydroxamic acid macrocycles using MTS. MTS relies on the formation of a metal−ligand supramolecular assembly in which the terminal amine and carboxylic acid groups of contiguous *endo*-HXA monomers are suitably positioned to allow ring closure upon in situ peptide coupling. This is designed to provide facile access to metal-loaded macrocycles (holomacrocycles), with apomacrocycles accessible upon incubation with a high concentration of chelator to compete for the templating metal ion (Scheme 3). The MTS reaction was conducted using a 1:2 Fe(III)/ligand stoichiometry, with in situ amide-bond-forming chemistry undertaken with DPPA and triethylamine.

The MTS reaction solution was analyzed using liquid chromatography−mass spectrometry (LC−MS), with selected ion monitoring (SIM) as the detection mode. The 1:2 Fe(III)/ligand stoichiometry was selected to promote the generation of dimeric macrocycles (Table 1). It was possible that the MTS system might generate trimeric macrocycles because this configuration would stabilize the octahedral coordination preference of Fe(III). The SIM values selected for the analysis correlated with the intrinsically charged dimeric Fe(III) macrocycle ($[M]^+$) and the protonated adduct ($[M + H]^+$) of the neutral trimeric Fe(III) macrocycle.

The signals in the LC trace were detected for each of **1a**−**6a** (Figure 1). Aside from the well-resolved and narrow signal for **5a**, these signals were broad and commonly contained a low-intensity shoulder, which could be due to the presence of a distribution of Fe(III) macrocycle conformers that were partially resolved by the LC conditions. The experimental MS isotope pattern at the peak maxima for **1a**−**6a** correlated well with the calculated isotope patterns (Figure 1, lower row). The LC signals were ascribed to the dimeric hydroxamic acid Fe(III) macrocycles, as determined from extraction ion chromatogram (EIC) measurements, which correlated strongly with the SIM traces (Figure S7, top and middle rows). EIC signals that corresponded with the $[M + H]^+$ adducts of the trimeric Fe(III) macrocycles were discernible only at baseline levels (Figure S7, lower row), which showed that the MTS reaction stoichiometry favored formation of the dimeric macrocycles. The signal for **5a** at m/z 518.2 was present with a signal at m/z 501.1 ascribable to the coelution of diphenyl hydrogen phosphate $[2M + H]^+$ as a product of DPPA-mediated peptide coupling.[46,47]

Production of Apomacrocycles 1b−6b. The MTS reaction solutions containing **1a**−**6a** were each treated with excess diethylenetriaminepentaacetic acid (DTPA) to compete for the Fe(III) template and liberate the corresponding apomacrocycles **1b**−**6b**. The LC signals for **1b**−**4b** and **6b** appeared as sharp, single peaks (Figure 2), with the experimental MS isotope patterns in agreement with the calculated data. The major MS signal correlated with the $[M + H]^+$ adduct of the neutral apomacrocycle, with lower-intensity signals present for sodium and potassium adducts. The solutions were analyzed for the presence of trimeric Fe(III)-free macrocycles, with minor peaks detected at <1% area of the dimeric analogues (Figure S8). In the case of **5b**, two well-resolved signals were observed at t_R = 30.2 min (peak 1) and t_R = 38.5 min (peak 2). The EIC data (Figure S8, middle row) showed that each peak was ascribable to a species with SIM 465. These two peaks were separated using semipreparative

DOI: 10.1021/acs.inorgchem.9b00878
Inorg. Chem. XXXX, XXX, XXX−XXX

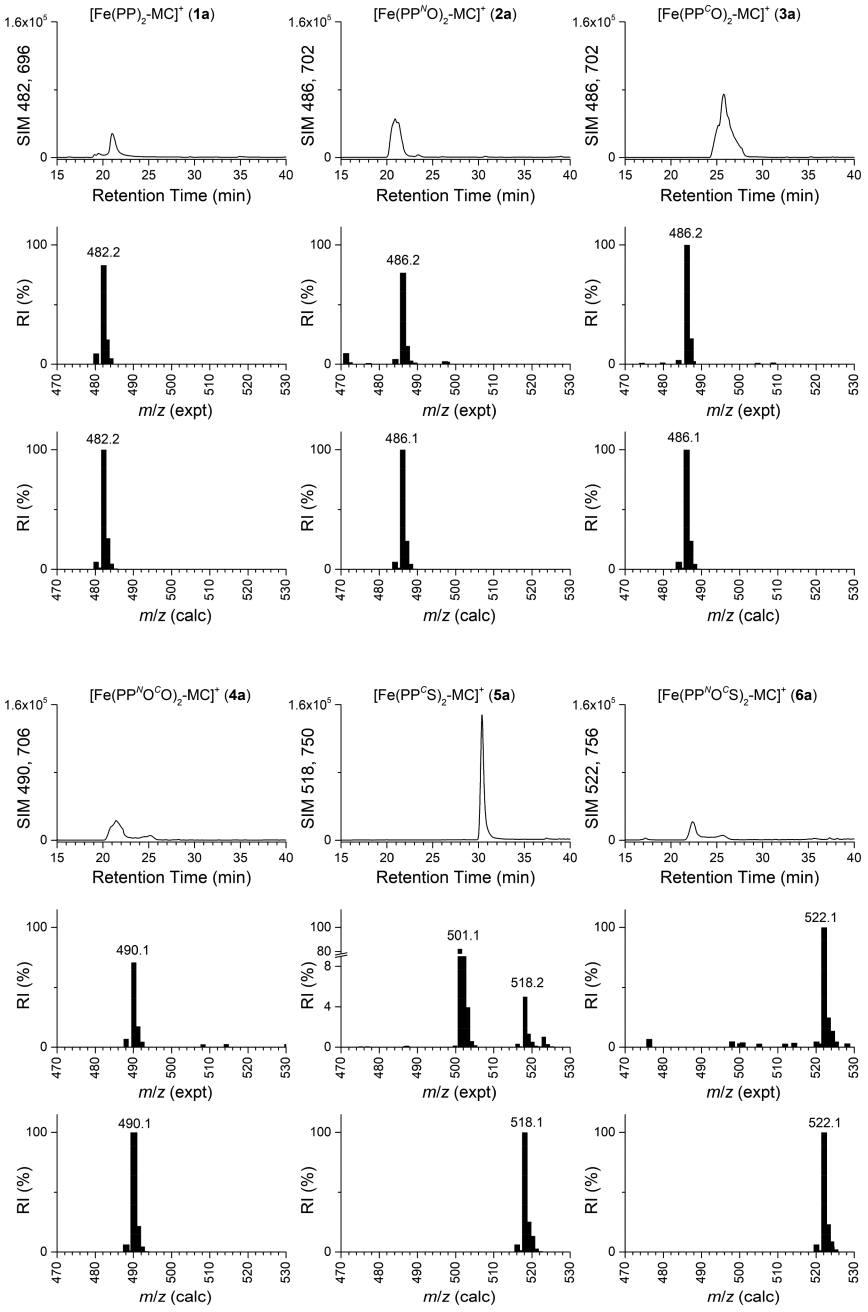

Figure 1. Complexes between Fe(III) and dimeric hydroxamic acid macrocycles (**1a**–**6a**) produced using MTS, as characterized using LC–MS (SIM detection; first row, **1a**–**3a**; fourth row, **4a**–**6a**), with the experimental or calculated isotope patterns shown in each corresponding column.

HPLC for further analysis (Figure S9). As expected, MS analysis of the separate solutions gave isotope patterns at 465.2 (peak 1) or 465.3 (peak 2). It was likely that one of these peaks was ascribable to **5b** and that the second peak was due to an artifact of the reaction and/or side product. The authenticity of **5b** was confirmed upon the addition of an aliquot of Fe(III) to each isolated solution. In the case of peak 1, the holomacrocycle **5a** was reconstituted (Figure S9e,g), while no LC signal was observed for **5a** from a solution of Fe(III) and peak 2 (Figure S9f). This identified peak 1 as the apomacrocycle **5b** and peak 2 as a species that had an *m*/*z* value coincident with **5b** but that was not relevant as a target. The species in peak 2 was present in the MTS mixture containing **5a**, as detected by EIC at 465 (Figure S9a, gray).

A more accurate comparison of the LC retention times for **1b**–**6b** was obtained from the LC trace from a mixture of apomacrocycles that had been isolated as individual fractions from the LC trace, with the authenticity of each compound shown using HRMS (Figures S10–S15). The LC trace from this composite solution (Figure 3a) showed a positive correlation between the *c* log *P* values and the LC retention times for **1b**–**6b** (r = 0.82 or 0.62 for *ACD/ChemSketch* or *Molinspiration* calculators, respectively; Figure 3b). The data points for **2b** and **3b** were the most significant outliers from the lines of best fit. Despite the presence of two ether oxygen atoms, which would be expected to increase the polarity, **3b** eluted in a less polar window than the methylene isostere **1b**. The apomacrocycle **4b**, which contained four ether oxygen atoms, eluted in the most polar region of the LC trace. The

DOI: 10.1021/acs.inorgchem.9b00878
Inorg. Chem. XXXX, XXX, XXX–XXX

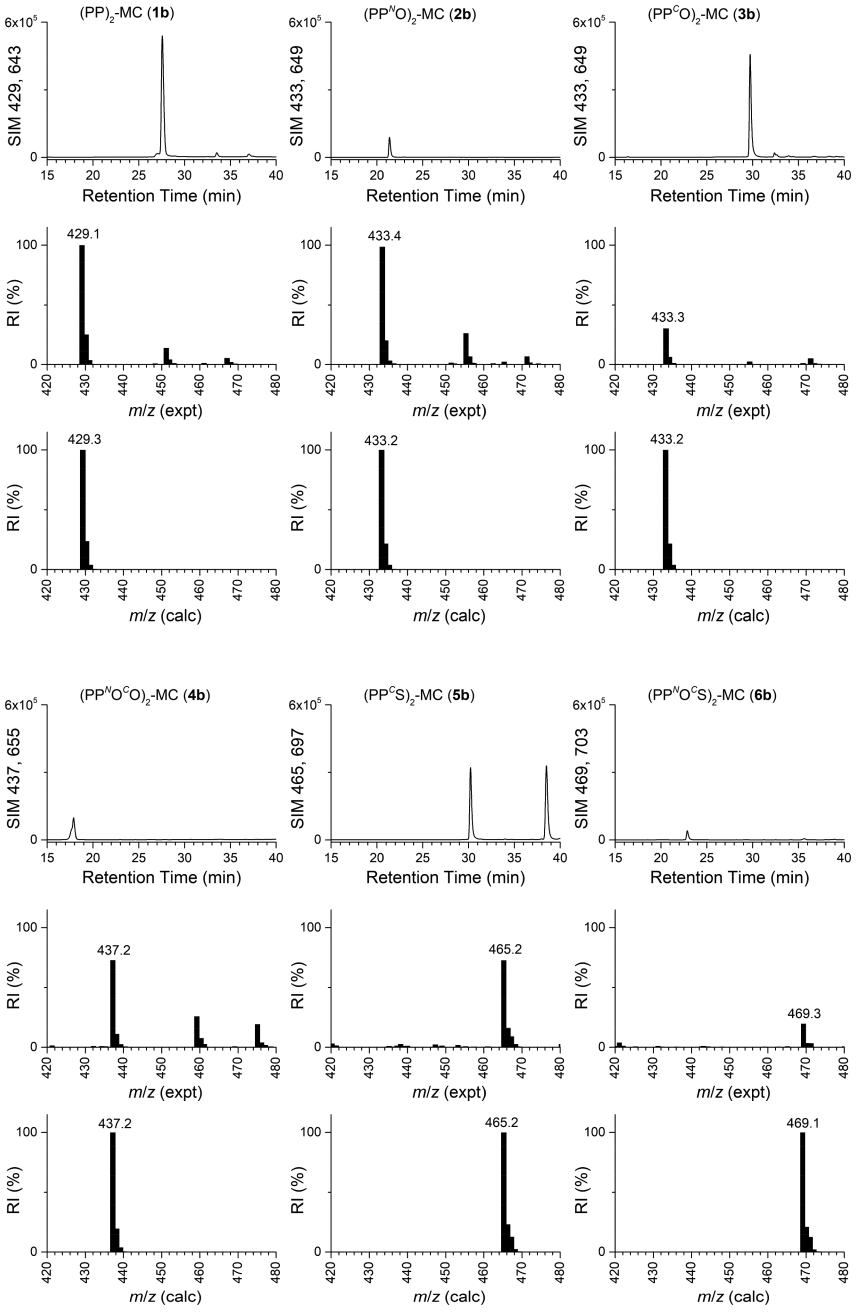

Figure 2. Dimeric hydroxamic acid apomacrocycles (**1b**–**6b**) detected upon removal of Fe(III) from **1a**–**6a**, as characterized using LC–MS (SIM detection; first row, **1b**–**3b**; fourth row, **4b**–**6b**), with the experimental or calculated isotope patterns shown in each corresponding column.

apomacrocycle **2b** eluted in the second most polar region of the LC trace and in a window significantly different from that of the isomer **3b**. This showed the position of the ether oxygen atom in the diamine-containing region (**2b**) or the dicarboxylic acid-containing region (**3b**) had a significant effect on the solvation properties, based on the surrogate measure of the LC retention time.

The rank order of the retention time of the holomacrocycles (lowest to highest), **2a** < **1a** < **4a** < **6a** < **3a** < **5a**, differed from that of the corresponding apomacrocycles (lowest to highest), **4b** < **2b** < **6b** < **1b** < **3b** < **5b** (Figure 3c). The apomacrocycle **1b** moved two places higher in the rank order compared to **1a**, while the apomacrocycle **4b** was ranked two places lower than **4a**. At a qualitative level, these trends suggest how the macrocycle properties might be modulated by the elements of structural diversity, including the type and location of backbone isosteres (methylene, oxygen, and sulfur) and the presence or absence of Fe(III).

^{1}H NMR Spectroscopy of the Apomacrocycle 1b. The scale and conversion efficiency of the MTS reaction using the standard amount of ∼4 mg of *endo*-HXA monomer produced **1b**–**6b** on an analytical scale. More material of **1b** was obtained from 10 in-parallel 1:2 Fe(III)/**1** MTS reaction solutions (Table S1), which were subject to in situ ring closure in the normal fashion. Each of the 10 reactions showed an intense signal in LC–MS at the SIM value corresponding with **1a** (SIM 482), which showed that the MTS reaction was robust and reproducible. The signal was coincident with a signal using visible detection at 450 nm, characteristic of Fe(III) siderophore complexes (Figure S16). The MTS

DOI: 10.1021/acs.inorgchem.9b00878
Inorg. Chem. XXXX, XXX, XXX–XXX

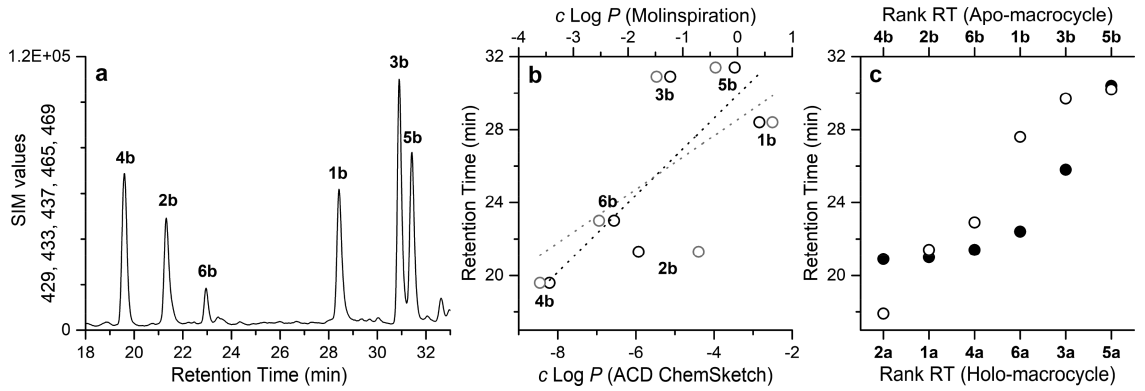

Figure 3. LC from a mixture of isolated solutions of **1b**–**6b** with detection using multiple SIM values (a), a plot of the *c* log *P* values of **1b**–**6b** from *ACD/ChemSketch* (black) or *Molinspiration* (gray) calculators versus retention time (b), and a plot of the rank order of the retention times of **1a**–**6a** (closed circles, bottom axis) and **1b**–**6b** (open circles, top axis) (c; using data from Figures 1 and 2).

reactions were pooled, purified, and treated with DTPA, with final purification generating about 1 mg of **1b** for ^{1}H NMR spectroscopy. The signals in the ^{1}H and ^{1}H–^{1}H COSY NMR spectra (Figures 4 and S17) were consistent with **1b** as a molecule with C_2 or C_i symmetry, with chemical shifts and multiplicities similar to those of regionally equivalent protons reported for putrebactin (Table 2 and Chart 2), which showed C_i symmetry by X-ray crystallography.[14]

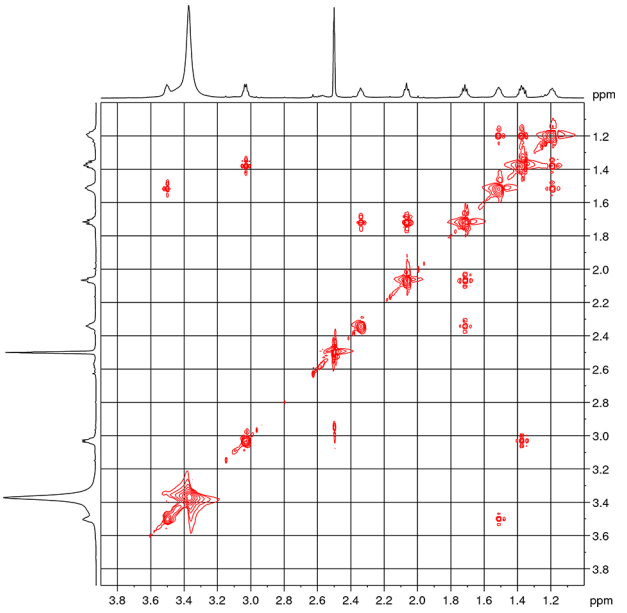

Figure 4. Expansion of ^{1}H–^{1}H COSY NMR spectrum (600 MHz, DMSO-d_6) of **1b**.

Chart 2. Numbering System for 1b and Putrebactin

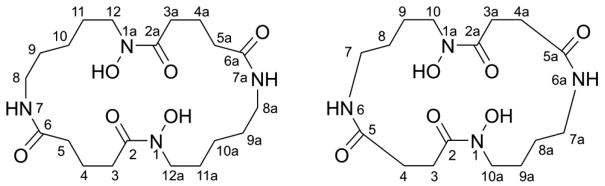

Density Functional Theory (DFT) Calculations of 1b–6b. DFT calculations were used to calculate selected molecular properties and estimate the solvation energetics of **1b**–**6b** (Table 3). Of most interest was to provide a rationale for the significant difference in the reverse-phase high-performance liquid chromatography (RP-HPLC) retention times observed by experiment for the constitutional isomers **2b** and **3b**. Although no symmetry constraints were imposed, all of the structures of **1b**–**6b** converged with pseudo-C_2 symmetry with the rotation axis positioned through the cavity of the macrocycle (Figure 5 and Tables S2–S7).

Analysis of the calculated molecular properties for **1b**–**6b** indicated **3b** as an outlier, particularly in terms of the

Table 2. ^{1}H NMR Spectroscopic Data for 1b and Putrebactin (DMSO-d_6)

(PP)$_2$-MC (**1b**)				putrebactin (ref 14)			
assignment[a]	δ_H	multiplicity	no.[b]	assignment[a]	δ_H	multiplicity	no.[b]
H-1(a)	9.47	s	2	H-1(a)	9.71	br	2
H-3(a)	2.07	t[c]	4	H-3(a)	2.26	t	4
H-4(a)	1.72	qn[c]	4	N/A			
H-5(a)	2.34	m[d]	4	H-4(a)	2.61	t	4
H-7(a)	7.70	s	2	H-6(a)	7.75	br	2
H-8(a)	3.04	m	4	H-7(a)	3.00	m	4
H-9(a)	1.38	m	4	H-8(a)	1.34	m	4
H-10(a)	1.20	m	4	N/A			
H-11(a)	1.51	qn[c]	4	H-9(a)	1.48	m	4
H-12(a)	3.50	m[d]	4	H-10(a)	3.47	t	4

[a]Atom numbering as per Chart 2. [b]Number of protons. [c]J = 7.1 Hz. [d]Triplet unresolved.

DOI: 10.1021/acs.inorgchem.9b00878
Inorg. Chem. XXXX, XXX, XXX–XXX

Table 3. Summary of the Calculated Molecular Properties and Solvation Energetics of 1b−6b

apomacrocycle		dipole moment, μ (D)	polarizability, μ (au)	cavity volume (Å^3)	cavity surface area (Å^2)	electronic spatial extent $\langle R^2 \rangle$ (au)	ΔH_{solv} (kJ mol^{-1})	ΔS_{solv} (J K^{-1} mol^{-1})	ΔG_{solv} (kJ mol^{-1})
$(PP)_2$-MC	**1b**	14.4	349	604	494	13103	−41.7	−41.7	−41.1
$(PP^NO)_2$-MC	**2b**	17.7	326	587	495	13070	−40.8	−36.6	−40.5
$(PP^CO)_2$-MC	**3b**	3.7	329	582	482	13040	−83.1	−83.7	−83.0
$(PP^NO^CO)_2$-MC	**4b**	15.2	305	561	465	12566	−62.1	−64.6	−61.1
$(PP^CS)_2$-MC	**5b**	13.0	374	613	496	14509	−87.1	−87.5	−86.9
$(PP^NO^CS)_2$-MC	**6b**	15.8	352	595	497	14340	−58.2	−59.8	−57.0

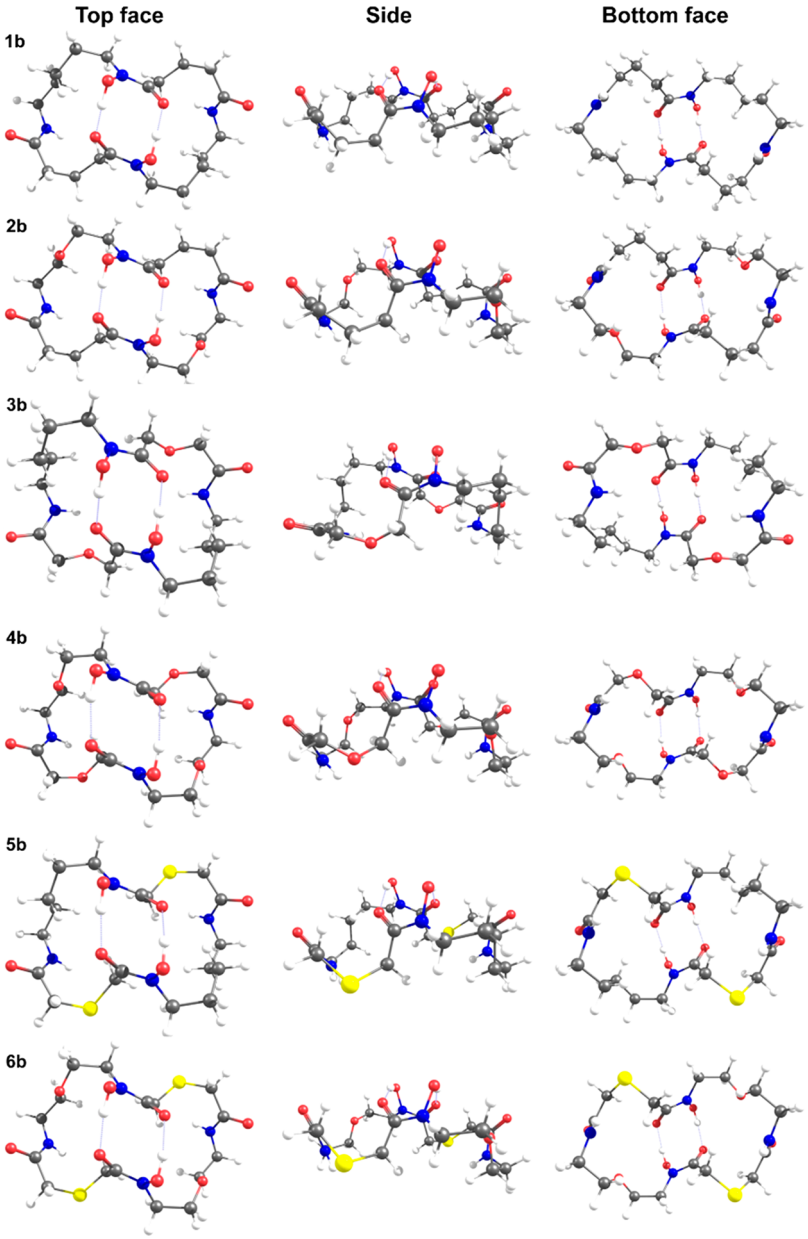

Figure 5. Three projections of the optimized structures of **1b−6b** calculated using the B3LYP/DGDZVP/PCM methodology.

calculated dipole moment. The calculated dipole moments (μ) of **1b**, **2b**, and **4b−6b** ranged between 13.0 and 17.7 D (Table 3), with the value for **3b** (μ = 3.7 D) showing a reduced polarity. Origins of this difference lie in the steric and electronic constraints imposed by inserting the ether group between the two carbonyl groups. In this position, the ether oxygen atom forces the amide groups to twist and point away from the macrocyclic cavity (essentially orthogonal to the pseudo-C_2 axis). In contrast to the other compounds in the series, this twist in **3b** reduces the polarity and dipole moment. The effect can be seen in the electrostatic potential (ESP) maps of **2b** and **3b** (Figure 6). No such difference was observed in the calculated properties or optimized structure of **5b**, which contains a thioether group in place of the ether

DOI: 10.1021/acs.inorgchem.9b00878
Inorg. Chem. XXXX, XXX, XXX−XXX

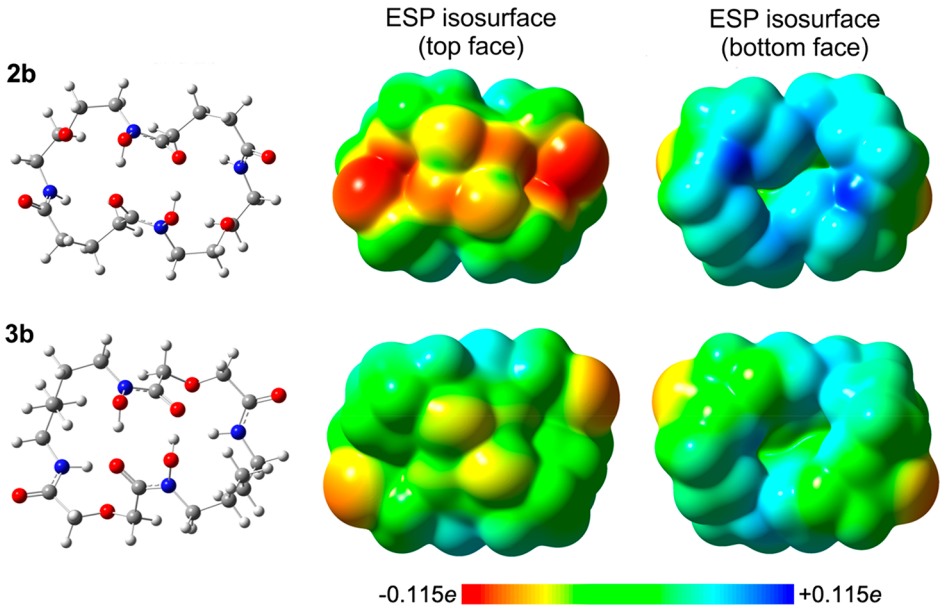

Figure 6. DFT-optimized structures of **2b** and **3b** and the calculated ESP maps (with charges in the range of −0.115e to 0.115e) showing projections from the top face (center), as viewed down the pseudo-C_2 rotation axis, and the opposing bottom face (right). ESPs are projected onto the total electron density isosurface (at the 99.9% cutoff). Structures were optimized using the B3LYP/DGDZVP methodology, and calculations included solvation effects in H_2O using a PCM.

group of **3b** (Figure S18). The larger sulfur atom in **5b** allows for increased conformational flexibility in the ring. Placing the ether group in the center of the diaminopentane-derived region in **2b** did not induce the same conformational restrictions, with **2b** retaining a high polarity. No discernible trend was observed in the calculated solvation energies (Table 3).

CONCLUSION

This work has reported a new synthesis for *endo*-HXA monomers that furnishes these ligands in higher yields (2−5 times greater) and in less time (3−4 times less) than previous methods. The use of the nosyl protecting group adds value to the synthesis through its orthogonality to other N-protecting groups and its removal under mild conditions. The amino alcohol reagent used in the first step allows an expansion of the structural diversity in *endo*-HXA monomers because of the ready availability of different analogues. The *endo*-HXA ligands **1**−**6** were used in successful MTS reactions in a 1:2 Fe(III)/ligand stoichiometry to produce in analytical yields the corresponding Fe(III)-loaded dimeric hydroxamic acid macrocycles **1a**−**6a**, which following treatment with DTPA, gave the apomacrocycles **1b**−**6b**. A total of 10 in-parallel MTS reactions using **1** gave sufficient apomacrocycle **1b** for characterization by ^{1}H NMR spectroscopy. Apomacrocycles **1b**−**6b** gave different retention times on an RP-HPLC column, which reflected different solvation properties ascribable to the presence and position of the methylene groups and ether and/or thioether atoms. The optimized structures and solvation properties of the ether-containing isomers **2b** and **3b** were examined by DFT calculations. The results confirmed that **3b** was anomalous in the series and that an ether group positioned between the carbonyl centers imposed steric and electronic constraints that invoked a twist in the macrocycle, which reduced the molecular polarity. Improved access to *endo*-HXA monomers could support MTS as a more robust method for generating metal-tailored macrocycles and other syntheses requiring these types of ligands. Mixed-ligand MTS conducted with 1 equiv of Fe(III) and a 1:1 ratio of two different monomers from **1**−**6** could provide access to 15 new dimeric hydroxamic acid macrocycles as a means to expand the structural diversity.

EXPERIMENTAL SECTION

All reactions were performed under an inert nitrogen atmosphere. The progress of the reactions was monitored by thin-layer chromatography (TLC), with plates visualized using UV light at 254 nm or by staining with ninhydrin, vanillin, or $FeCl_3$. ^{1}H and ^{13}C NMR spectroscopy was performed on a Bruker 600 MHz AVIIII with a TCI cryoprobe at 25 °C operating with *Topspin* 3.5 NMR software. Samples were made to a concentration of 10 mg mL^{-1} in $CDCl_3$ (Sigma-Aldrich, 99.8%), CD_3OD (Cambridge Isotope Laboratory, 99.8%), or dimethyl sulfoxide (DMSO)-d_6 (Cambridge Isotope Laboratory, 99.9%). Chemical shifts are reported in ppm relative to the residual solvent peaks ($CDCl_3$, δ_H 7.27 ppm, δ_C 77.23 ppm; CD_3OD, δ_H 3.31 ppm, δ_C 49.00 ppm; DMSO-d_6, δ_H 2.50 ppm, δ_C 39.52 ppm). Signal multiplicities are labeled as s (singlet), d (doublet), t (triplet), q (quartet), qn (quintet), or m (multiplet). Coupling constants are designated as J (Hz). Two-dimensional ^{1}H−^{1}H COSY and ^{1}H−^{13}C HSQC NMR spectra of **1b** were obtained using a Shigemi tube (DMS-005TB, Shigemi Inc., Japan). High-resolution mass spectrometry (HRMS) was conducted on a Bruker SolariX 2XR 7T Fourier transform ion cyclotron mass spectrometer at the School of Chemistry, University of Sydney.

General Procedures. *Reagents.* 1-Amino-5-pentanol (95%), 2-(2-aminoethoxy)ethanol (98%), 1,8-diazabicyclo[5.4.0]undec-7-ene (DBU; 98%), dichloromethane (DCM; ≥99.8%), 1,4-dioxane-2,6-dione (common name: diglycolic anhydride, 95%), diisopropyl azodicarboxylate (DIAD; 99%), diphenylphosphoryl azide (DPPA; 97%), di-*tert*-butyl dicarbonate (99%), glutaric anhydride (95%), iron(III) acetylacetonate (97%), triethylamine (Et_3N; ≥99%), methanol (MeOH; 99.8%), 2-mercaptoethanol (≥99%), *N*,*N*-dimethylformamide (DMF; 99.8%), succinic anhydride (≥99%), tetrahydrofuran (THF; ≥99%), *tert*-butyl alcohol (≥99.5%), and trifluoroacetic acid (TFA; 99%) were purchased from Sigma-Aldrich (Castle Hill, Australia). Hexane and ethyl acetate were purchased from Thermofisher Scientific (Sydney, Australia). 1,4-Oxathiane-2,6-dione (thiodiacetic anhydride, 98%) was purchased from Fluorochem

DOI: 10.1021/acs.inorgchem.9b00878
Inorg. Chem. XXXX, XXX, XXX−XXX

(Hadfield, United Kingdom). All solvents were anhydrous unless stated otherwise. All chemicals were used as received. Milli-Q H_2O was used for all experiments, as required.

Instrumentation. Silica Chromatography. Flash chromatography was performed on a Grace Reveleris X2 autoflash system using hexane and ethyl acetate as solvents, unless specified otherwise. The cartridge sizes and flow rates were varied depending on the scale of the reaction: 0.1−1 g scale reaction (cartridge = 12 g; flow rate = 30 mL min^{-1}) and 1−8 g scale reaction (cartridge = 40 g; flow rate = 40 mL min^{-1}). Methods were developed using the Reveleris autogradient feature based on R_f values from TLC experiments. Crude compounds were dissolved in a minimum amount of ethyl acetate and injected onto the column via the injection port.

Reverse-Phase Liquid Chromatography−Mass Spectrometry (RP-LC−MS). RP-LC−MS was employed using an Agilent Technologies HPLC system (Santa Clara, CA) consisting of an autoinjector (100 μL loop), an Agilent 1260 Infinity degasser, a quaternary pump, and an Agilent 6120 series quadrupole electrospray ionization (ESI) mass spectrometer. An Agilent C18 column reverse-phase prepacked column (4.6 × 150 mm i.d.; particle size 5 μm) was used for all experiments. An Agilent OpenLAB Chromatography Data System ChemStation Edition was used to process mass chromatograms in each of the scans and the SIM or EIC detection modes. Samples were made to a concentration of 1 mg mL^{-1} in MeOH or for MTS samples in 1:1 DMF/H_2O. The following instrumental conditions were used: flow rate, 0.5 mL min^{-1}; injection volume, 5 μL; spray voltage, 4 kV; capillary voltage, 3 kV; capillary temperature, 250 °C; tube lens offset, 10 V. Mobile phases were prepared by mixing acetonitrile (ACN) formic acid (99.9:0.1, mobile phase B) and H_2O/formic acid (99.9:0.1, mobile phase A). Method A: 0−100% ACN/H_2O gradient over 40 min. Method B: 0−28% ACN/H_2O gradient over 40 min.

Semipreparative HPLC Purification of ***1b****.* Semipreparative HPLC was conducted on a Shimadzu LC-20 series LC system with two LC-20AP pumps, a SIL-10AP autosampler, an SPD-20A UV/vis detector, a FRC-10A fraction collector, and a Shimadzu ShimPack GIS-C18 column (150 × 10.0 mm i.d.; 5 mL min^{-1}; particle size 5 μm). Shimadzu LabSolutions Software (version 5.73) was used for data acquisition and processing. Mobile phase A: aqueous TFA (0.05%). Mobile phase B: ACN/TFA (99.95/0.05%).

H-Cube. Hydrogenation was performed on an H-cube Mini Plus with a HPLC micropump. The 10% Pd/C CatCart was from ThalesNano (ID: THS-01111). The mobile phase was prepared by mixing *tert*-butyl alcohol/ethyl acetate (9:1). The method used a temperature of 60 °C and a flow rate of 1 mL min^{-1} with a run time of 20 min.

General Methods. *MTS.* The purity of **1**−**6** was sufficient to proceed to MTS without the need for resource and time-intensive preparative HPLC. A MeOH solution (1 mL) containing **1** (4.1 mg, 17.6 μmol) was added to a MeOH solution (1 mL) containing $Fe(acac)_3$ (3.1 mg, 8.8 μmol) to give a 2 mg mL^{-1} solution with respect to **1**. The solution was stirred for 2 h, the solvent was removed in vacuo, and the product was dried under high vacuum overnight. DMF (4 mL) was added to the crude mixture, followed by the addition of DPPA (29 μL, 35.2 μmol) and Et_3N (10.7 μL, 35.2 μmol). The reaction mixture was stirred for 5 days, and aliquots of 100 μL were taken from the mixture and diluted with Milli-Q H_2O (100 μL) to quench the reaction. Analogous procedures were conducted for **2**−**6**. Reaction mixtures were analyzed by LC−MS (positive ion) using total ion chromatogram, SIM, and EIC detection modes.

Removing Fe(III) from Holomacrocycles ***1a***−***6a****.* An aliquot of the reaction mixture (100 μL) was taken and diluted with an equivalent aliquot of DTPA (0.2 M), and the mixture was left to incubate at room temperature (rt) overnight. A sample was taken and analyzed by LC−MS.

Isolation of the Analytical Yields of Apomacrocycles ***1b***−***6b*** *by HPLC.* The MTS solutions treated with DTPA-containing **1b**−**6b** were purifed by HPLC (method B) and analyzed by HRMS. Fractions were collected over the following elution times: **1b** (26−30 min), **2b** (19−23 min), **3b** (27−31 min), **4b** (15−19 min), **5b** (peak 1, 28−32 min; peak 2, 36−40 min), **6b** (20−24 min). The ACN was removed via rotary evaporation, and the fractions were then lyophilized to dryness. The solid residue was redissolved in 200 μL of H_2O, and the solutions were pooled and analyzed by LC−MS and HRMS (Figures S10−S15).

In-Parallel MTS Reactions To Prepare ***1b*** *for* ^{1}*H NMR Spectroscopy.* A total of 10 in-parallel MTS reactions were conducted using Fe(III)/**1** in a 1:2 ratio, with masses of **1** ranging between 3.7 and 15.2 mg (Table S1). After 5 days, the formation of **1a** was confirmed using LC−MS (Figure S16), and the reactions were pooled and concentrated in vacuo. The concentrate was then diluted in 5 mL of H_2O and semipurified by a Waters C-18 SPE cartridge (2 g). The filtrate was concentrated in vacuo and further diluted with a 0.2 M DTPA solution (5 mL). The mixture was subjected to semi-preparative HPLC, with a gradient of 2−40% solvent B in solvent A from 0 to 30 min. The product eluted at 20.3 min. Fractions containing the product were pooled and lyophilized to yield **1b** (∼1 mg) characterized by NMR spectroscopy. ^{1}H NMR (600 MHz, DMSO-d_6): δ_H 9.47 (s, 2H, H-1(a)), 7.70 (s, 2H, H-7(a)), 3.50 (m, 4H, H-12(a)), 3.04 (m, 4H, H-8(a)), 2.34 (m, 4H, H-5(a)), 2.07 (t, J = 7.1 Hz, 4H, H-3(a)), 1.72 (qn, J = 7.1 Hz, 4H, H-4(a)), 1.51 (m, 4H, H-11(a)), 1.38 (qn, J = 7.1 Hz, 4H, H-9(a)), 1.20 (m, 4H, H-10(a)) (refer to Chart 2 for atom numbering). ^{13}C NMR (150 MHz, DMSO-d_6): δ_C 46.1, 37.9, 33.0, 29.9, 28.2, 25.3, 22.9, 20.4 (by ^{1}H−^{13}C HSQC; shifts for quaternary carbon atoms not determined). LRMS (ESI$^+$): m/z 429.3 ([M + H]$^+$, 100%), 451.3 ([M + Na]$^+$, 5%). HRMS. Calcd for $C_{20}H_{36}N_4O_6$ + Na ([M + Na]$^+$): m/z 451.25271. Found: m/z 451.25290.

Synthesis. *O-Benzyl-N-(2-nitrophenylsulfonyl)hydroxylamine.* The N,O-bis-protected hydroxylamine reagents were prepared in a previous work[43] and used in the synthesis of hydroxamic acid-based compounds, including DFOB.[44] The NH group in these reagents is sufficiently acidic (pK_a 5.1) for use in the Mitsunobu reaction. The nosyl protecting group was used in the synthesis of linear hydroxamic acids and the preparation of other types of ligands for radiochemistry.[43−45] *O*-Benzylhydroxylamine hydrochloride (5.0 g, 31.3 mmol) was dissolved in anhydrous pyridine (60 mL), stirred vigorously, and cooled to −5 °C. A solution of 2-nitrobenzylsulfonyl chloride (7.1 g, 32.0 mmol) in pyridine (20 mL) was added dropwise. The solution was left to stir at −5 °C for 30 min, then allowed to warm to rt and stirred for a further 2 h. H_2O (15 mL) was added to terminate the reaction, and the solvents were removed in vacuo. The residue was redissolved in EtOAc/H_2O (1:1, 400 mL) and partitioned in a separatory funnel. The organic layer was washed with 5% HCl, H_2O, and $NaHCO_3$ (200 mL each). The organic layer was concentrated *in vacuo* to yield the semipure product as an orange crystalline solid (6.9 g, 70%). ^{1}H NMR (600 MHz, $CDCl_3$): δ_H 8.24−8.26 (m, 1H), 8.12 (s, 1H), 7.78−7.88 (m, 3H), 7.37 (s, 5H), 5.10 (s, 2H). ^{13}C NMR (150 MHz, $CDCl_3$): δ_C 149.1, 135.6, 135.3, 132.5, 130.3, 129.7, 128.5, 124.6, 78.7. LRMS (ESI$^+$): m/z 309.2 ([M + H]$^+$, 100%). The data are consistent with the literature.[43]

O-tert-Butyl-N-(2-nitrophenylsulfonyl)hydroxylamine. O-tert-Butylhydroxylamine hydrochloride (5.06 g, 40.2 mmol) was dissolved in anhydrous $CHCl_3$ (80 mL) and the reaction cooled to −5 °C. Et_3N (11.7 mL, 84.4 mmol) was added dropwise, followed by the dropwise addition of a solution of 2-nitrobenzylsulfonyl chloride (8.93, 40.2 mmol) in $CHCl_3$ (50 mL). The reaction was stirred at −5 °C for 2 h, warmed to rt, and left to stir overnight. The reaction mixture was washed with H_2O, 1 M HCl, H_2O, 5% $NaHCO_3$, H_2O, and brine (40 mL each). The organic layer was concentrated *in vacuo* to yield the product as a yellow crystalline solid (8.82 g, 80%). ^{1}H NMR (600 MHz, $CDCl_3$): δ_H 8.15−8.16 (m, 1H), 7.78−7.86 (m, 3H), 1.26 (s, 9H). ^{13}C NMR (150 MHz, $CDCl_3$): δ_C 148.5, 134.5, 133.8, 133.7, 132.7, 125.3, 82.9, 26.7. LRMS (ESI$^+$): m/z 275.1 ([M + H]$^+$, 100%). The data are consistent with the literature.[43]

*N-Boc-1-amino-5-pentanol (****7****).* To a solution of 1-amino-5-pentanol (1.50 g, 14.5 mmol) in CH_2Cl_2 (120 mL) was added a solution of Boc_2O (3.16 g, 14.5 mmol) in CH_2Cl_2 (10 mL). The solution was treated with Et_3N (2.22 mL, 15.9 mmol) dropwise, and

DOI: 10.1021/acs.inorgchem.9b00878
Inorg. Chem. XXXX, XXX, XXX−XXX

the mixture was stirred at rt for 4 h. The reaction was concentrated *in vacuo*, and the crude product was purified using autoflash chromatography (gradient: 30% EtOAc over 2 min, 30−60% over 5 min, and 60% over 2 min) to afford the product as a yellow oil (90%). ^{1}H NMR (600 MHz, $CDCl_3$): δ_H 3.67 (t, J = 6.5 Hz, 2H), 3.20 (d, J = 6.2 Hz, 2H), 1.63 (qn, J = 7.2 Hz, 2H), 1.56 (qn, J = 7.3 Hz, 2H), 1.49 (s, 9H), 1.42−1.46 (m, 2H). ^{13}C NMR (150 MHz, $CDCl_3$): δ_C 156.1, 77.1, 62.3, 40.4, 32.2, 29.8 28.4, 22.9. LRMS (ESI$^+$): m/z 226.1 ([M + Na]$^+$, 100%). The data are consistent with the literature.[48]

*N-Boc-2-(2-aminoethoxy)ethanol (**8**).* To a solution of 2-(2-aminoethoxy)ethanol (1.52 g, 14.5 mmol) in CH_2Cl_2 (120 mL) was added a solution of Boc_2O (3.16 g, 14.5 mmol) in CH_2Cl_2 (10 mL). The solution was treated with Et_3N (2.22 mL, 15.9 mmol) dropwise, and the mixture was stirred at rt for 4 h. The reaction was concentrated *in vacuo*, and the crude product was purified using autoflash chromatography (gradient: 30% EtOAc over 2 min, 30−60% over 5 min, and 60% over 2 min) to afford the product as a yellow oil (90%). ^{1}H NMR (600 MHz, $CDCl_3$): δ_H 5.21 (s, 1H), 3.67−3.69 (m, 2H), 3.49−3.53 (m, 4H), 3.26−3.29 (m, 2H), 1.40 (s, 9H). ^{13}C NMR (150 MHz, $CDCl_3$): δ_C 156.3, 79.1, 72.2, 70.1, 61.2, 40.2, 28.4. LRMS (ESI$^+$): m/z 228.1 ([M + Na]$^+$, 100%). The data are consistent with the literature.[49]

*N,O-Bis-protected Hydroxylamine Compounds **13**−**16**.* To a solution of **7** (1.50 g, 7.38 mmol) or **8** (1.51 g, 7.38 mmol) in THF (15 mL) was added *O-tert*-butyl-*N*-(2-nitrophenylsulfonyl)-hydroxylamine (2.03 g, 7.38 mmol) or *O*-benzyl-*N*-(2-nitrophenylsulfonyl)hydroxylamine (2.25 g, 7.38 mmol) and PPh_3 (5.80 g, 22.14 mmol). After stirring for 15 min, the reaction was cooled to 0 °C, and DIAD (4.48 mL, 22.14 mmol) was added dropwise. The mixture was stirred for 30 min, then heated to 40 °C, and stirred for 8 h. The reaction was concentrated *in vacuo*, diluted with diethyl ether, cooled to 0 °C, and stirred until a precipitate formed. The mixture was filtered, and the filtrate was concentrated *in vacuo* and purified using autoflash chromatography (gradient: 9% EtOAc over 1 min, 9−28% over 10 min, and 28% over 2 min) to furnish the semipure nosyl-protected amine compound (**9**−**12**) as an orange oil. Products **9**−**12** were not further characterized and were used directly in the next step of the synthesis. The product was redissolved in DMF (10 mL) and treated with 2-mercaptoethanol (517 μL, 7.38 mmol) and DBU (1.12 mL, 7.38 mmol), and the solution was stirred at rt for 3 h. The reaction was concentrated *in vacuo*, diluted with H_2O, and extracted with CH_2Cl_2. The crude mixture was purified using autoflash chromatography (gradient: 10% EtOAc over 2 min, 10−25% over 4 min, and 25% over 5 min) to yield **13**−**16** as a yellow oil (75% over two steps).

*tert-Butyl [5-(tert-butoxyamino)pentyl]carbamate (**13**).* ^{1}H NMR (600 MHz, $CDCl_3$): δ_H 3.22 (d, J = 7.2 Hz, 2H), 2.94 (t, J = 7.1 Hz, 2H), 1.58 (qn, J = 6.2 Hz, 4H), 1.54 (s, 9H), 1.43−1.47 (m, 2H), 1.28 (s, 9H). ^{13}C NMR (150 MHz, $CDCl_3$): δ_C 155.9, 79.0, 77.2, 52.8, 40.5, 30.0, 28.4, 27.0, 26.8, 24.5. LRMS (ESI$^+$): m/z 275.3 ([M + H]$^+$, 100%).

*tert-Butyl [2-[2-(tert-Butoxyamino)ethoxy]ethyl]carbamate (**14**).* ^{1}H NMR (600 MHz, $CDCl_3$): δ_H 3.53 (t, J = 5.1 Hz, 4H), 3.48 (d, J = 4.6 Hz, 2H), 3.28 (s, 2H), 2.97 (t, J = 5.1, 2H), 1.55 (s, 9H), 1.29 (s, 9H). ^{13}C NMR (150 MHz, $CDCl_3$): δ_C 156.0, 76.8, 69.8, 67.1, 60.4, 52.5, 40.3, 28.4, 26.7. LRMS (ESI$^+$): m/z 277.2 ([M + H]$^+$, 100%).

*tert-Butyl [5-[(Benzyloxy)amino]pentyl]carbamate (**15**).* ^{1}H NMR (600 MHz, $CDCl_3$): δ_H 7.26−7.32 (m, 5H), 4.67 (s, 2H), 3.07 (s, 2H), 2.89 (t, J = 7.1 Hz, 2H), 1.49 (qn, J = 7.5 Hz, 2H), 1.42−1.45 (m, 2H), 1.41 (s, 9H), 1.30 (qn, J = 7.7 Hz, 2H). ^{13}C NMR (150 MHz, $CDCl_3$): δ_C 171.2, 137.9, 128.4, 128.3, 127.7, 77.4, 76.1, 51.9, 40.4, 29.9, 28.4, 27.0, 24.3. LRMS (ESI$^+$): m/z 309.2 ([M + H]$^+$, 100%).

*tert-Butyl [2-[2-[(Benzyloxy)amino]ethoxy]ethyl]carbamate (**16**).* ^{1}H NMR (600 MHz, $CDCl_3$): δ_H 7.26−7.33 (m, 5H), 4.69 (s, 2H), 3.58 (t, J = 5.1 Hz, 2H), 3.55 (t, J = 4.8 Hz, 2H), 3.28 (d, J = 4.6 Hz, 2H), 3.06 (t, J = 5.1 Hz, 2H), 1.42 (s, 9H). ^{13}C NMR (150 MHz, $CDCl_3$): δ_C 156.0, 137.9, 128.4, 128.3, 127.8, 79.2, 76.0, 70.0, 67.2, 51.5, 40.4, 28.4. LRMS (ESI$^+$): m/z 311.2 ([M + H]$^+$, 100%).

*Glutarylated N,O-Bis-protected Hydroxylamine Compounds **17**−**22**.* A further improvement was gained in the reaction step with the anhydride (Scheme 2, step iv) by replacing pyridine with dichloromethane and triethylamine. The triethylamine base was subsequently determined to be unnecessary. These modifications mitigated the high variability in yields (40−80%) and reduced the reaction time for this step from 24 to 3 h. To a solution of **13** (401 mg, 1.46 mmol), **14** (404 mg, 1.46 mmol), **15** (450 mg, 1.46 mmol), or **16** (453 mg, 1.46 mmol) in CH_2Cl_2 (10 mL) was added either glutaric anhydride (167 mg, 1.46 mmol), 1,4-dioxane-2,6-dione (169 mg, 1.46 mmol), or 1,4-oxathiane-2,6-dione (193 mg, 1.46 mmol). The mixture was stirred at rt for 3 h, concentrated *in vacuo*, and purified using autoflash chromatography (gradient: 29% EtOAc over 2 min, 29−61% over 7 min, and 61% over 4 min) to afford the product as a white solid (**17**, **21**, and **22**) or a clear oil (**18**−**20**; 85%).

*5-[tert-Butoxy[5-[(tert-butoxycarbonyl)amino]pentyl]amino]-5-oxopentanoic Acid (**17**).* ^{1}H NMR (600 MHz, $CDCl_3$): δ_H 2.41 (qn, J = 7.4 Hz, 4H), 1.93 (qn, J = 7.0 Hz, 4H), 1.60 (t, J = 7.1 Hz, 2H), 1.46−1.47 (m, 2H), 1.41 (s, 9H), 1.27 (s, 9H), 1.23 (t, J = 7.1 Hz, 4H). ^{13}C NMR (150 MHz, $CDCl_3$): δ_C 178.0, 171.3, 82.7, 79.2, 60.4, 40.4, 33.2, 32.9, 29.6, 28.4, 23.9, 21.0, 19.8, 19.6, 14.2. LRMS (ESI$^+$): m/z 411.3 ([M + Na]$^+$, 100%).

*11-(tert-Butoxy)-2,2-dimethyl-4,12-dioxo-3,8-dioxa-5,11-diazahexadecan-16-oic Acid (**18**).* ^{1}H NMR (600 MHz, $CDCl_3$): δ_H 3.75 (s, 2H), 3.56 (s, 4H), 3.34 (s, 2H), 2.50 (t, J = 7.0 Hz, 2H), 2.03 (t, J = 7.0 Hz, 2H), 1.53 (s, 9H), 1.39 (s, 9H). ^{13}C NMR (150 MHz, $CDCl_3$): δ_C 177.9, 156.2, 79.3, 69.7, 66.2, 50.5, 40.3, 33.1, 32.1, 28.4, 27.6, 19.9. LRMS (ESI$^+$): m/z 413.2 ([M + Na]$^+$, 100%).

*11-(Benzyloxy)-2,2-dimethyl-4,12-dioxo-3,14-dioxa-5,11-diazahexadecan-16-oic Acid (**19**).* ^{1}H NMR (600 MHz, $CDCl_3$): δ_H 7.33−7.42 (m, 5H), 4.80 (s, 2H), 4.20 (s, 2H), 4.01 (s, 2H), 3.71 (s, 2H), 3.10 (s, 2H), 1.68 (qn, J = 7.3 Hz, 2H), 1.50 (qn, J = 7.4 Hz, 2H), 1.43 (s, 9H), 1.32 (s, 2H). ^{13}C NMR (150 MHz, $CDCl_3$): δ_C 172.5, 165.6, 133.7, 129.7, 129.6, 129.5, 129.0, 128.9, 76.2, 45.4, 40.3, 29.6, 28.4, 26.4, 26.2, 24.7, 22.8. LRMS (ESI$^+$): m/z 447.2 ([M + Na]$^+$, 100%).

*11-(Benzyloxy)-2,2-dimethyl-4,12-dioxo-3,8,14-trioxa-5,11-diazahexadecan-16-oic Acid (**20**).* ^{1}H NMR (600 MHz, $CDCl_3$): δ_H 7.39−7.45 (m, 5H), 4.91 (s, 2H), 4.31 (s, 2H), 4.20 (s, 2H), 4.10 (s, 2H), 3.66 (t, J = 5.1 Hz, 2H), 3.49 (t, J = 5.6 Hz, 2H), 3.20 (t, J = 5.5 Hz, 2H), 1.40 (s, 9H). ^{13}C NMR (150 MHz, $CDCl_3$): δ_C 172.2, 157.0, 134.5, 129.5, 128.8, 128.4, 78.7, 76.1, 69.4, 68.1, 67.6, 66.2, 60.1, 39.9, 27.4, 24.9. LRMS (ESI$^+$): m/z 449.2 ([M + Na]$^+$, 100%).

*11-(tert-Butoxy)-2,2-dimethyl-4,12-dioxo-3-oxa-14-thia-5,11-diazahexadecan-16-oic Acid (**21**).* ^{1}H NMR (600 MHz, $MeOD_4$): δ_H 3.82 (s, 2H), 3.52 (s, 2H), 3.13 (t, J = 7.0 Hz, 2H), 1.56−1.59 (m, 2H), 1.53 (s, 9H), 1.44 (s, 9H), 1.37−1.41 (m, 4H). ^{13}C NMR (150 MHz, $MeOD_4$): δ_C 172.2, 83.5, 77.9, 77.7, 77.5, 51.7, 48.8, 33.4, 33.3, 33.1, 32.9, 29.2, 27.0, 24.6. LRMS (ESI$^+$): m/z 429.2 ([M + Na]$^+$, 100%).

*11-(tert-Butoxy)-2,2-dimethyl-4,12-dioxo-3,8-dioxa-14-thia-5,11-diazahexadecan-16-oic Acid (**22**).* ^{1}H NMR (600 MHz, $CDCl_3$): δ_H 3.73 (s, 4H), 3.56 (s, 2H), 3.38 (s, 2H) 3.32 (s, 2H), 1.50 (s, 9H), 1.39 (s, 9H). ^{13}C NMR (150 MHz, $CDCl_3$): δ_C 173.2, 156.5, 89.9, 79.7, 69.8, 66.0, 50.2, 49.6, 40.3, 33.9, 33.7, 28.3, 27.6. LRMS (ESI$^+$): m/z 431.2 ([M + Na]$^+$, 100%).

*endo-HXA Monomers **1**−**6**.* A solution of **17** (427 mg, 1.1 mmol), **18** (429 mg, 1.1 mmol), **21** (447 mg, 1.1 mmol), or **22** (449 mg, 1.1 mmol) was prepared in CH_2Cl_2/TFA (1:9, 5 mL), and the solution was stirred at rt for 4 h. The mixture was concentrated, redissolved in toluene, and concentrated *in vacuo*. H_2O was added, and the product was lyophilized, yielding an orange gum. The corresponding *endo*-HXA ligand **1**, **2**, **5**, or **6** was left as a TFA salt until further reaction was required (95%). A solution of **19** (467 mg, 1.1 mmol) or **20** (469 mg, 1.1 mmol) was prepared in *tert*-butyl alcohol/ethyl acetate (9:1, 18 mL) at a concentration of 50 mM and subject to hydrogenation using a H-cube Mini Plus. The collected solution was concentrated *in vacuo*, and the compound was redissolved in CH_2Cl_2/TFA (9:1, 5 mL) and reacted for 2 h. The mixture was concentrated, redissolved in toluene, and concentrated *in vacuo*. H_2O was added, and the

DOI: 10.1021/acs.inorgchem.9b00878
Inorg. Chem. XXXX, XXX, XXX−XXX

solution was lyophilized to yield an orange gum. The corresponding *endo*-HXA ligand **3** or **4** was left as a TFA salt until further reaction was required (95%).

*5-[(5-Aminopentyl)(hydroxy)amino]-5-oxopentanoic Acid (PPH) (**1**).* ^{1}H NMR (600 MHz, $MeOD_4$): δ_H 3.63 (t, J = 6.9 Hz, 2H, H-9), 2.92 (t, J = 7.2 Hz, 2H, H-6), 2.55 (t, J = 6.6 Hz, 2H, H-2), 2.35 (t, J = 7.2 Hz, 2H, H-11), 1.86−1.90 (qn, J = 7.0 Hz, 2H, H-10), 1.68 (t, J = 7.0 Hz, 4H, H-3,5), 1.38−1.40 (m, 2H, H-4). ^{13}C NMR (150 MHz, $MeOD_4$): δ_C 175.4, 173.9, 39.2, 32.5, 30.9, 26.5, 25.7, 22.9, 19.9, 19.8. LRMS (ESI$^+$): m/z 233.1 ([M + H]$^+$, 100%). HRMS: Calcd for $C_{10}H_{21}N_2O_4$ ([M + H]$^+$): m/z 233.14958. Found: m/z 233.14954.

*5-[[2-(2-Aminoethoxy)ethyl](hydroxy)amino]-5-oxopentanoic Acid (PPH^{N}O, **2**).* ^{1}H NMR (600 MHz, DMSO-d_6): δ_H 7.81 (bs, 2H, NH_3·TFA, H-1), 3.69 (t, J = 5.9 Hz, 2H, H-6), 3.59 (t, J = 5.9 Hz, H-3), 3.58 (m, J = 5.2 Hz, H-5), 2.95 (q, J = 5.1 Hz, 2H, H-2), 2.40 (t, J = 7.2 Hz, 2H, H-11), 2.24 (t, J = 7.4 Hz, 2H, H-9), 1.70 (qn, J = 7.3 Hz, 2H, H-10). ^{13}C NMR (150 MHz, DMSO-d_6): δ_C 174.3 (C-8), 172.9 (C-12), 66.4 (C-3, -5), 46.8 (C-6), 38.6 (C-2), 33.0 (C-9), 30.9 (C-11), 20.0 (C-10). LRMS (ESI$^+$): m/z 235.1 ([M + H]$^+$, 100%). HRMS: Calcd for $C_9H_{19}N_2O_5$ ([M + H]$^+$): m/z 235.12885. Found: m/z 235.12867.

*2-[2-[(5-Aminopentyl)(hydroxy)amino]-2-oxoethoxy]acetic Acid (PPH^{C}O, **3**).* ^{1}H NMR (600 MHz, DMSO-d_6): δ_H 7.75 (bs, 2H, NH_3·TFA, H-1), 4.32 (s, 2H, H-9), 4.10 (s, 2H, H-11), 3.47 (t, J = 6.8 Hz, 2H, H-6), 2.73−2.78 (m, 2H, H-2), 1.51−1.56 (m, 4H, H-3,5), 1.27 (qt, J = 7.4 Hz, 2H, H-4). ^{13}C NMR (150 MHz, DMSO-d_6): δ_C 171.4 (C-8), 169.3 (C-12), 67.6 (C-9), 67.2 (C-11), 46.9 (C-6), 38.7 (C-2), 26.7 (C-3, -5), 25.6 (C-4). LRMS (ESI$^+$): m/z 235.1 ([M + H]$^+$, 100%). HRMS: Calcd for $C_9H_{19}N_2O_5$ ([M + H]$^+$): m/z 235.12885. Found: m/z 235.12882.

*2-[2-[[2-(2-Aminoethoxy)ethyl](hydroxy)amino]-2-oxoethoxy]-acetic Acid (PPH^{N}O^{C}O, **4**).* ^{1}H NMR (600 MHz, DMSO-d_6): δ_H 7.82 (bs, 2H, NH_3·TFA, H-1), 4.08 (d, J = 6.4 Hz, 4 H, H-9, -11), 3.66 (t, J = 5.4 Hz, 2H, H-6), 3.59 (t, J = 5.8 Hz, 2H, H-5), 3.58 (t, J = 5.6 Hz, 2H, H-3) 2.95−2.96 (m, 2H, H-2). ^{13}C NMR (150 MHz, DMSO-d_6): δ_C 171.2 (C-8), 169.9 (C-12), 67.5 (C-9), 67.2 (C-11), 66.3 (C-3), 66.0 (C-5), 46.9 (C-6), 38.6 (C-2). LRMS (ESI$^+$): m/z 237.1 ([M + H]$^+$, 100%). HRMS: Calcd for $C_8H_{17}N_2O_6$ ([M + H]$^+$): m/z 237.10811. Found: m/z 237.10803.

*2-[[2-[(5-Aminopentyl)(hydroxy)amino]-2-oxoethyl]thio]acetic Acid (PPH^{C}S) (**5**).* ^{1}H NMR (600 MHz, DMSO-d_6): δ_H 7.69 (bs, 2H, NH_3·TFA, H-1), 3.54 (s, 2H, H-9), 3.49 (t, J = 6.7 Hz, 2H, H-6), 3.34 (s, 2H, H-11; peak coincident with the H_2O peak; analyzed by HSQC), 2.75−2.76 (m, 2H, H-2), 1.53 (t, J = 7.1 Hz, 4H, H-3, -5), 1.27 (t, J = 7.1 Hz, 2H, H-4). ^{13}C NMR (150 MHz, DMSO-d_6): δ_C 170.9 (C-8), 168.7 (C-12), 47.0 (C-6), 38.7 (C-2), 33.4 (C-11), 32.6 (C-9), 26.6 (C-3, -5), 25.6 (C-4). LRMS (ESI$^+$): m/z ([M + H]$^+$, 100%). HRMS: Calcd for $C_9H_{19}N_2O_4S$ ([M + H]$^+$): m/z 251.10600. Found: m/z 251.10565.

*2-[[2-[[2-(2-Aminoethoxy)ethyl](hydroxy)amino]-2-oxoethyl]-thio]acetic Acid (PPH^{N}O^{C}S) (**6**).* ^{1}H NMR (600 MHz, DMSO-d_6): δ_H 7.76 (bs, 2H, NH_3·TFA, H-1), 3.70 (t, J = 5.6 Hz, 2H, H-6), 3.56−3.62 (m, 8H, H-3, -5, -9, -11), 2.96 (s, 2H, H-2). ^{13}C NMR (150 MHz, DMSO-d_6): δ_C 170.9 (C-8), 169.3 (C-12), 66.3 (C-3, -5), 46.9 (C-6), 38.6 (C-2), 32.6 (C-9, -11). LRMS (ESI$^+$): m/z 253.1 ([M + H]$^+$, 100%). HRMS: Calcd for $C_8H_{17}N_2O_5S$ ([M + H]$^+$): m/z 253.08527. Found: m/z 253.08501.

Computational Details. All calculations were conducted using DFT, as implemented in the *Gaussian16*, revision A.03, suite of ab initio quantum chemistry programs. Normal self-consistent-field and geometry convergence criteria were employed throughout, and the structures were optimized without using symmetry constraints. All structures were optimized in the gas phase and in solution phase using a polarizable continuum model (PCM) and the B3LYP/DGDZVP methodology. Solvated phase calculations were implemented using the SCRF keyword with default parameters and selecting H_2O as the solvent (dielectric constant, ε = 78.3553). Harmonic frequency analysis based on analytical second derivative was used to characterize optimized structures as local minima. The choice of the solvation model reflects our standard aqueous phase conditions employed in the potential use and application of the macrocyclic chelates described in this work. Optimized structures were analyzed by using *Chemcraft* (version 1.8, build 536b) and *GaussView 6.0.16* (Gaussian Inc., Wallingford, MA). ESP maps (calculated in the range −0.115e to +0.115e) were mapped onto the total electron density surface (set to a cutoff of 99.9% density).

■ ASSOCIATED CONTENT

Supporting Information

The Supporting Information is available free of charge on the ACS Publications website at DOI: 10.1021/acs.inorgchem.9b00878.

Additional data for **1**−**6** and **1b**, including NMR spectroscopy and HRMS (PDF)

■ AUTHOR INFORMATION

Corresponding Author

*Tel.: +61 2 9351 6738. E-mail: rachel.codd@sydney.edu.au (R.C.).

ORCID

Michael P. Gotsbacher: 0000-0002-7153-1250
Jason P. Holland: 0000-0002-0066-219X
Rachel Codd: 0000-0002-2703-883X

Notes

The authors declare no competing financial interest.

■ ACKNOWLEDGMENTS

This work was supported by the Australian Research Council (Grant DP140100092) and the Australian Government Research Training Program Scholarship scheme (to C.J.M.B.). A. Sresuthasan is acknowledged for useful discussions.

■ REFERENCES

(1) Albrecht-Gary, A.-M.; Crumbliss, A. L. In *Metal Ions in Biological Systems*; Sigel, A., Sigel, H., Eds.; Marcel Dekker, Inc.: New York, 1998; Vol. 35, pp 239−327.

(2) Butler, A. Iron acquisition: straight up and on the rocks? *Nat. Struct. Mol. Biol.* **2003**, *10*, 240−241.

(3) Raymond, K. N.; Dertz, E. A. In *Iron Transport in Bacteria*; Crosa, J. H., Mey, A. R., Payne, S. M., Eds.; ASM Press: Washington, DC, 2004; pp 3−17.

(4) Hider, R. C.; Kong, X. Chemistry and biology of siderophores. *Nat. Prod. Rep.* **2010**, *27*, 637−657.

(5) Kurth, C.; Kage, H.; Nett, M. Siderophores as molecular tools in medical and environmental applications. *Org. Biomol. Chem.* **2016**, *14*, 8212−8227.

(6) Johnstone, T. C.; Nolan, E. M. Beyond iron: non-classical biological functions of bacterial siderophores. *Dalton Trans.* **2015**, *44*, 6320−6339.

(7) Miethke, M. Molecular strategies of microbial iron assimilation: from high-affinity complexes to cofactor assembly systems. *Metallomics* **2013**, *5*, 15−28.

(8) Sandy, M.; Butler, A. Microbial iron acquisition: Marine and terrestrial siderophores. *Chem. Rev.* **2009**, *109*, 4580−4595.

(9) Chu, B. C.; Garcia-Herrero, A.; Johanson, T. H.; Krewulak, K. D.; Lau, C. K.; Peacock, R. S.; Slavinskaya, Z.; Vogel, H. J. Siderophore uptake in bacteria and the battle for iron with the host; a bird's eye view. *BioMetals* **2010**, *23*, 601−611.

(10) Schalk, I. J.; Hannauer, M.; Braud, A. New roles for bacterial siderophores in metal transport and tolerance. *Environ. Microbiol.* **2011**, *13*, 2844−2854.

(11) Codd, R.; Richardson-Sanchez, T.; Telfer, T. J.; Gotsbacher, M. P. Advances in the chemical biology of desferrioxamine B. *ACS Chem. Biol.* **2018**, *13*, 11−25.

DOI: 10.1021/acs.inorgchem.9b00878
Inorg. Chem. XXXX, XXX, XXX−XXX

(12) Dhungana, S.; White, P. S.; Crumbliss, A. L. Crystal structure of ferrioxamine B: A comparative analysis and implications for molecular recognition. *JBIC, J. Biol. Inorg. Chem.* **2001**, *6*, 810−818.
(13) van der Helm, D.; Poling, M. The crystal structure of ferrioxamine E. *J. Am. Chem. Soc.* **1976**, *98*, 82−86.
(14) Ledyard, K. M.; Butler, A. Structure of putrebactin, a new dihydroxamate siderophore produced by *Shewanella putrefaciens*. *JBIC, J. Biol. Inorg. Chem.* **1997**, *2*, 93−97.
(15) Böttcher, T.; Clardy, J. A chimeric siderophore halts swarming. *Angew. Chem., Int. Ed.* **2014**, *53*, 3510−3513.
(16) Soe, C. Z.; Pakchung, A. A. H.; Codd, R. Directing the biosynthesis of putrebactin or desferrioxamine B in *Shewanella putrefaciens* through the upstream inhibition of ornithine decarboxylase. *Chem. Biodiversity* **2012**, *9*, 1880−1890.
(17) Winkelmann, G.; Schmid, D. G.; Nicholson, G.; Jung, G.; Colquhoun, D. J. Bisucaberin - a dihydroxamate siderophore isolated from *Vibrio salmonicida*, an important pathogen of farmed Atlantic salmon (*Salmo salar*). *BioMetals* **2002**, *15*, 153−160.
(18) Soe, C. Z.; Telfer, T. J.; Levina, A.; Lay, P. A.; Codd, R. Simultaneous biosynthesis of putrebactin, avaroferrin and bisucaberin by *Shewanella putrefaciens* and characterisation of complexes with iron(III), molybdenum(VI) or chromium(V). *J. Inorg. Biochem.* **2016**, *162*, 207−215.
(19) Takahashi, A.; Nakamura, H.; Kameyama, T.; Kurasawa, S.; Naganawa, H.; Okami, Y.; Takeuchi, T.; Umezawa, H.; Iitaka, Y. Bisucaberin, a new siderophore, sensitizing tumor cells to macrophage-mediated cytolysis. II. Physico-chemical properties and structure determination. *J. Antibiot.* **1987**, *40*, 1671−1676.
(20) Nishio, T.; Tanaka, N.; Hiratake, J.; Katsube, Y.; Ishida, Y.; Oda, J. Isolation and structure of the novel dihydroxamate siderophore alcaligin. *J. Am. Chem. Soc.* **1988**, *110*, 8733−8734.
(21) Codd, R.; Soe, C. Z.; Pakchung, A. A. H.; Sresutharsan, A.; Brown, C. J. M.; Tieu, W. The chemical biology and coordinaton chemistry of putrebactin, avaroferrin, bisucaberin, and alcaligin. *JBIC, J. Biol. Inorg. Chem.* **2018**, *23*, 969−982.
(22) Pakchung, A. A. H.; Soe, C. Z.; Lifa, T.; Codd, R. Complexes formed in solution between vanadium(IV)/(V) and the cyclic dihydroxamic acid putrebactin or linear suberodihydroxamic acid. *Inorg. Chem.* **2011**, *50*, 5978−5989.
(23) Soe, C. Z.; Pakchung, A. A. H.; Codd, R. Dinuclear $[V^{V}O(putrebactin))_2(\mu\text{-}OCH_3)_2]$ formed in solution as established from LC-MS measurements using ^{50}V-enriched V_2O_5. *Inorg. Chem.* **2014**, *53*, 5852−5861.
(24) Bergeron, R. J.; McManis, J. S. The total synthesis of bisucaberin. *Tetrahedron* **1989**, *45*, 4939−4944.
(25) Driggers, E. M.; Hale, S. P.; Lee, J.; Terrett, N. K. The exploration of macrocycles for drug discovery - an underexploited structural class. *Nat. Rev. Drug Discovery* **2008**, *7*, 608−624.
(26) Giordanetto, F.; Kihlberg, J. Macrocyclic drugs and clinical candidates: What can medicinal chemists learn from their properties? *J. Med. Chem.* **2014**, *57*, 278−295.
(27) Ardi, V. C.; Alexander, L. D.; Johnson, V. A.; McAlpine, S. R. Macrocycles that inhibit the binding between heat shock protein 90 and TPR-containing proteins. *ACS Chem. Biol.* **2011**, *6*, 1357−1366.
(28) Marti-Centelles, V.; Pandey, M. D.; Burguete, M. I.; Luis, S. V. Macrocyclization reactions: the importance of conformational, configurational, and template-induced preorganisation. *Chem. Rev.* **2015**, *115*, 8736−8834.
(29) Dougherty, P. G.; Qian, Z.; Pei, D. Macrocycles as protein-protein interaction inhibitors. *Biochem. J.* **2017**, *474*, 1109−1125.
(30) Cummings, M. D.; Sekharan, S. Structure-based macrocycle design in small-molecule drug discovery and simple metrics to identify opportunities for macrocyclization of small-molecule ligands. *J. Med. Chem.* **2019**, DOI: 10.1021/acs.jmedchem.8b01985.
(31) Sresutharsan, A.; Tieu, W.; Richardson-Sanchez, T.; Soe, C. Z.; Codd, R. Dimeric and trimeric homo- and heteroleptic hydroxamic acid macrocycles formed using mixed-ligand Fe(III)-based metal-templated synthesis. *J. Inorg. Biochem.* **2017**, *177*, 344−351.
(32) Kachadourian, R.; Chuilon, S.; Mérienne, C.; Kunesch, G.; Deroussent, A. A new total synthesis of ferrioxamine E through metal-templated cyclic trimerization. *Supramol. Chem.* **1997**, *8*, 301−308.
(33) Lifa, T.; Tieu, W.; Hocking, R. K.; Codd, R. Forward and reverse (*retro*) iron(III)- or gallium(III)-desferrioxamine E and ring-expanded analogs prepared using metal-templated synthesis from *endo*-hydroxamic acid monomers. *Inorg. Chem.* **2015**, *54*, 3573−3583.
(34) Tieu, W.; Lifa, T.; Katsifis, A.; Codd, R. Octadentate zirconium(IV)-loaded macrocycles with varied stoichiometry assembled from hydroxamic acid monomers using metal-templated synthesis. *Inorg. Chem.* **2017**, *56*, 3719−3728.
(35) Wencewicz, T. A.; Oliver, A. G.; Miller, M. J. Iron(III)-templated macrolactonization of trihydroxamate siderophores. *Org. Lett.* **2012**, *14*, 4390−4393.
(36) Holland, J. P.; Divilov, V.; Bander, N. H.; Smith-Jones, P. M.; Larson, S. M.; Lewis, J. S. ^{89}Zr-DFO-J591 for immunoPET of prostate-specific membrane antigen expression *in vivo*. *J. Nucl. Med.* **2010**, *51*, 1293−1300.
(37) Holland, J. P.; Vasdev, N. Charting the mechanism and reactivity of zirconium oxalate with hydroxamate ligands using density functional theory: Implications in new chelate design. *Dalton Trans.* **2014**, *43*, 9872−9884.
(38) Bergeron, R. J.; Liu, Z.-R.; McManis, J. S.; Wiegand, J. Structural alterations in desferrioxamine compatible with iron clearance in animals. *J. Med. Chem.* **1992**, *35*, 4739−4744.
(39) Kadi, N.; Oves-Costales, D.; Barona-Gómez, F.; Challis, G. L. A new family of ATP-dependent oligomerization-macrocyclization biocatalysts. *Nat. Chem. Biol.* **2007**, *3*, 652−656.
(40) Izawa, T.; Mukaiyama, T. The partial reduction of carboxylic acids to aldehydes *via* 3-acylthiazolidine-2-thiones with diisobutylaluminum hydride and with lithium tri-tert-butoxyaluminum hydride. *Bull. Chem. Soc. Jpn.* **1979**, *52*, 555−558.
(41) Bergeron, R. J.; Pegram, J. J. An efficient total synthesis of desferrioxamine B. *J. Org. Chem.* **1988**, *53*, 3131−3134.
(42) Rütschlin, S.; Böttcher, T. Dissecting the mechanism of oligomerization and macrocyclization reactions of NRPS-independent siderophore synthetases. *Chem. - Eur. J.* **2018**, *24*, 16044−16051.
(43) Reddy, P. A.; Schall, O. F.; Wheatley, J. R.; Rosik, L. O.; McClurg, J. P.; Marshall, G. R.; Slomczynska, U. *O*-Protected *N*-(2-nitrophenylsulfonyl)hydroxylamines: Novel reagents for the synthesis of hydroxamates. *Synthesis* **2001**, *2001*, 1086−1092.
(44) Poreddy, A. R.; Schall, O. F.; Osiek, T. A.; Wheatley, J. R.; Beusen, D. D.; Marshall, G. R.; Slomczynska, U. Hydroxamate-based iron chelators: Combinatorial syntheses of desferrioxamine B analogues and evaluation of binding affinities. *J. Comb. Chem.* **2004**, *6*, 239−254.
(45) Price, E. W.; Zeglis, B. M.; Cawthray, J. F.; Lewis, J. S.; Adam, M. J.; Orvig, C. What a difference a carbon makes: H_4octapa vs H_4C3octapa, ligands for In-111 and Lu-177 radiochemistry. *Inorg. Chem.* **2014**, *53*, 10412−10431.
(46) Shioiri, T.; Ninomiya, K.; Yamada, S. Diphenylphosphoryl azide. A new convenient reagent for a modified Curtus reaction and for the peptide synthesis. *J. Am. Chem. Soc.* **1972**, *94*, 6203−6205.
(47) Montalbetti, C. A. G. N.; Falque, V. Amide bond formation and peptide coupling. *Tetrahedron* **2005**, *61*, 10827−10852.
(48) Szabo, M.; Klein Herenbrink, C.; Christopoulos, A.; Lane, J. R.; Capuano, B. Structure-activity relationships of privileged structures lead to the discovery of novel biased ligands at the dopamine D2 receptor. *J. Med. Chem.* **2014**, *57*, 4924−4939.
(49) Singh, V.; Wang, S.; Kool, E. T. Genetically encoded multispectral labeling of proteins with polyfluorophores on a DNA backbone. *J. Am. Chem. Soc.* **2013**, *135*, 6184−6191.

DOI: 10.1021/acs.inorgchem.9b00878
Inorg. Chem. XXXX, XXX, XXX−XXX